Linear stability of optimal streaks in the log-layer of turbulent channel flows

Frédéric Alizard[a)]
Laboratoire DynFluid, Arts et Métiers ParisTech and CNAM, 151 Boulevard de l'Hopital, 75013 Paris, France

The importance of secondary instability of streaks for the generation of vortical structures attached to the wall in the logarithmic region of turbulent channels is studied. The streaks and their linear instability are computed by solving equations associated with the organized motion that include an eddy-viscosity modeling the effect of incoherent fluctuations. Three friction Reynolds numbers, Re_τ = 2000, 3000, and 5000, are investigated. For all flow cases, optimal streamwise vortices (i.e., having the highest potential for linear transient energy amplification) are used as initial conditions. Due to the lift-up mechanism, these optimal perturbations lead to the nonlinear growth of streaks. Based on a Floquet theory along the spanwise direction, we observe the onset of streak secondary instability for a wide range of spanwise wavelengths when the streak amplitude exceeds a critical value. Under neutral conditions, it is shown that streak instability modes have their energy mainly concentrated in the overlap layer and propagate with a phase velocity equal to the mean streamwise velocity of the log-layer. These neutral log-layer modes exhibit a sinuous pattern and have characteristic sizes that are proportional to the wall distance in both streamwise and spanwise directions, in agreement with the Townsend's attached eddy hypothesis (A. Townsend, the structure of turbulent shear flow, Cambridge university press, 1976 2nd edition). In particular, for a distance from the wall varying from $y^+ \approx 100$ (in wall units) to $y \approx 0.3h$, where h is half the height of the channel, the neutral log-layer modes are self-similar with a spanwise width of $\lambda_z \approx y/0.3$ and a streamwise length of $\lambda_x \approx 3\lambda_z$, independently of the Reynolds number. Based on this observation, it is suggested that compact vortical structures attached to the wall can be ascribed to streak secondary instabilities. In addition, spatial distributions of fluctuating vorticity components show that the onset of secondary instability is associated with the roll-up of the shear layer at the edge of the low-speed streak, similarly to a three-dimensional mixing layer

I. INTRODUCTION

Since the pioneer work of Theodorsen[1] on horseshoes vortices, significant progress towards the understanding of wall-turbulence has come to light with the analysis of organized motions also called eddies or coherent structures.[2,3] These motions can be seen as elementary bricks of wall-turbulence and they exhibit a remarkable degree of persistence and regularity, i.e., they possess temporal and spatial coherence. Due to their large contribution to momentum transport, production of kinetic energy, and time-averaged statistics,[4,5] the kinematic properties of such motions (for instance the spatial scales and the rotational aspect) and dynamic properties (for instance, the temporal scale and the stability properties) are all of fundamental interest.

Consistent with the logarithmic dependence of the mean velocity profile on wall distance, Townsend[6] proposes that characteristic lengths of coherent structures that populate the logarithmic region scale with their distance from the wall. In that sense, he defined these structures as "attached

a)Electronic mail: frederic.alizard@cnam.fr.

to the wall." Townsend[6] suggests that these structures are geometrically self-similar and contribute strongly to the Reynolds stress in the overlap region. The same author also argues that streamwise and spanwise turbulence intensities are logarithmic functions when they are expressed in terms of the wall-normal coordinate. A self-similar hierarchical model for attached coherent structures is further emphasized by Perry and Chong[7] by means of flow visualization techniques. According to the spectral attached-eddy model of Perry *et al.*,[8] in the intermediate region, the streamwise energy spectrum is supposed to have an α^{-1} dependence where α is the wavenumber in the streamwise direction.

As underlined by Marusic *et al.*,[9] the major difficulty when studying the logarithmic zone is that the mean velocity profile deviates slightly from a logarithmic behavior, especially at low Reynolds numbers. To unravel the Reynolds number effect, Marusic *et al.*[9] carry out statistical analyses on experimental database of turbulent boundary layers and pipe flows at high Reynolds numbers. Marusic *et al.*[9] give, thus, strong evidence that turbulence intensities (streamwise and spanwise) exhibit a universal logarithmic behavior consistently with the Townsend-Perry attached-eddy model. Regarding the scaling proposed by Perry *et al.*,[8] Nickels *et al.*[10] give experimental evidence for the α^{-1} law associated with the overlap region of turbulent boundary layers at high Reynolds numbers.

With the increase of computational power, numerical simulations are now feasible at Reynolds numbers comparable to those of experiments. For instance, Sillero *et al.*[11] and Lee and Moser[12] present results of direct numerical simulations (DNS) of turbulent boundary layers and turbulent channel flows, respectively, in the range of $Re_\tau = 2000$–5000 where Re_τ denotes the friction Reynolds number. The authors show that the variance of the spanwise velocity component is seen to be a logarithmically decreasing function with the distance from the wall although the streamwise component behaves differently. At intermediate distances from the wall, a region where the streamwise energy spectrum exhibits an α^{-1} dependence is also recently observed in DNS by Lee and Moser.[12]

Despite the convincing agreement between the Townsend-Perry attached-eddy model and the turbulent statistics, the relationship between statistics and the dynamics of coherent structures remains to be unraveled. In that respect, the understanding of the organization and space-time dynamics of coherent motions has made much progress during the last decades using the "minimal flow unit" approach, which allows individual flow features to evolve in relative isolation from one another.[13] For instance, numerical simulations in periodic domains of "minimal" dimensions show that wavy low-velocity streaks with a characteristic spanwise spacing of approximately 100 wall units and quasi-streamwise vortices in the buffer region of wall-bounded flow are related to each other and are self-sustaining (Jiménez and Moin,[14] Hamilton *et al.*,[15] Waleffe,[16] and Panton[17] for a review). However, minimal flow simulations fail to properly describe the nature of those relations and the physical process at the origin of the amplification of coherent motions.

The mean profiles of wall-bounded turbulent flows are known to be linearly stable (asymptotically) but there have been several attempts to relate their coherent structures to a linear transient growth mechanism. In this context, although turbulence requires the nonlinearity of the Navier-Stokes equations, the essential role of the linear transient growth in maintaining near-wall turbulence is clearly enlightened by Kim and Lim.[18] Using numerical simulations, they show that without the linear coupling term representing the transfer from wall-normal velocity to wall-normal vorticity (the so-called lift-up effect[19]), near-wall turbulence cannot be sustained.

Within the framework of the optimal linear transient growth theory,[20] del Alamo and Jiménez,[21] Cossu *et al.*,[22] and Pujals *et al.*[23] investigate the temporal linear stability of the organized part of the motion (i.e., decorrelated of the incoherent background turbulence[24]) in channels and turbulent boundary layers with turbulent mean velocity profiles and turbulent eddy viscosities. They show that the most amplified structures in the inner-region correspond to wall-layer streaks with characteristic spanwise length scales that are consistent with numerical and experimental observations: $\lambda_z^+ \approx 100$ wall units (see Jiménez and Moin[14] and Kline *et al.*,[4] for instance). The above analyses confirm previous results of Butler and Farrel[25] that highlight the important role of linear transient growth in describing the streaks near the wall. In addition, they give further support to the use of linearized equations about the mean flow for describing organized motions in wall bounded turbulent flows. The condition for linearization about the mean flow is recently discussed by Jiménez.[26]

Concerning the regeneration of near-wall streamwise vortices, Schoppa and Hussain[27] investigate scenarios that involve streaks secondary instability. In particular, those authors highlight the signifi-

cant limitation of vortex regeneration scenarios based on normal-mode streaks instability and suggest a mechanism that involves a secondary transient growth. Furthermore, structural approaches that rely upon minimal flow simulations and stability theories have also led to the observation that bursting events in the buffer region are strongly associated with the destabilization of streamwise streaks.

More recently, Flores and Jiménez[13] extend the minimal simulation boxes to the logarithmic region. They show that the energy-containing motion in the intermediate layer exhibits a behavior similar to the one observed in the buffer layer. For a given distance from the wall, the minimal box contains a segment of velocity streak and a vortex cluster. In particular, the flow in the minimal box undergoes quasi-periodic bursts during which the streak experiences a wavy oscillation and a subsequent break-up of its structure. They also show that the bursting period scales with the distance from the wall and the height of the minimal box increases linearly with its spanwise size, in agreement with the attached-eddy concept developed by Townsend.[6] The recent study of Jiménez[28] provides a review on coherent motions in minimal simulation boxes associated with the logarithmic region.

Hwang and Cossu[29] further confirm that the process by which wall-attached eddies are self-sustained exhibit similarities with near-wall dynamics. In particular, they illustrate that coherent structures mainly located in the logarithmic layer survive when motions at smaller scales are artificially removed. They also observed that these motions have geometrically similar characteristics in agreement with the attached-eddy model. More recently, Hwang[30] shows that attached-eddies are grouped into two distinct elements: a long streaky structure that is dominated by streamwise velocity fluctuations and more compact vortical structures carrying all the velocity components (referenced as vortex clusters by del Alamo *et al.*[31]). These compact vortical structures are also observed experimentally by Tomkins and Adrian[32] and Marusic and Hutchins.[33]

For the origin of streaks, there is now strong evidence that a linear transient growth mechanism plays also an important role in the logarithmic layer. Using a similar approach, del Alamo and Jiménez,[21] Hwang and Cossu,[34] Moarref *et al.*[35] for a turbulent channel flow, and Alizard *et al.*[36] for supersonic turbulent boundary layers show that linear optimal modes in the logarithmic region exhibit a geometrically self-similar behavior since their wall-parallel length scales are proportional to their height. Furthermore, optimal modes display strong similarities with wall-layer streaks indicating that they also grow under the action of a lift-up mechanism. In addition, Moarref *et al.*[35] show that a necessary condition for the existence of geometrically self-similar optimal modes is the presence of a logarithmic turbulent mean velocity.

While all these results seem to clearly establish the link between the first element of an attached eddy (i.e., the streak) and the linear optimal transient growth, less is known about the second element (i.e., vortex clusters). Experimental studies of turbulent boundary layers conducted by Tomkins and Adrian[32] show that the spanwise size of vortices varies linearly with distance from the wall in the logarithmic region. The authors suggest that the growth of vortices is consistent with the vortex packets model where these packets are groups of hairpin vortices. Recently, Sharma and McKeon[37] proposed a model for the emergence of hairpin packets in the log-layer using a suitable combination of optimal modes.

Apart from this hypothesis, del Alamo *et al.*,[31] Hwang and Cossu,[29] and Hwang[30] suggest that a streamwise low-speed streak and vortex clusters aligned to this structure can be interpreted as two dynamically mutually dependent motions of a single attached eddy. It is recently suggested by Park *et al.*[38] that large-scale motions (**LSMs**) in the outer region (having $\lambda_z \approx O(\delta)$ with δ the outer length scale) can be caused by an instability of very large scale motions, (**VLSMs**, i.e., long streaky structures having $\lambda_z \approx O(10\delta)$). By considering idealized streaks of turbulent channel flows, they show the existence of an unstable sinuous mode if the streak amplitude exceeds a certain threshold. In particular, both the shape of the unstable mode and its streamwise extent exhibit some agreement with large-scale motions in the outer region. Similarly, it has been recently conjectured that, in the logarithmic region, vortex clusters could also be related to an instability of streamwise streaks.[30] From the above discussion, it seems clear that the origin of compact vortical structures attached to the wall is currently a matter of debate.

The main goal of this work is to investigate whether streaks associated with the log-layer of turbulent channels may experience a modal instability and to highlight its connection with the emergence of compact vortical structures that populate the logarithmic region. In particular, the success of Park

et al.[38] to predict the origin of large scale motions in the outer region has led us to develop a similar strategy in the intermediate layer. Then, we will also address some fundamental issues: Is the unstable mode associated with the streak instability attached to the wall? Does the streak become unstable to a sinuous mode rather than a varicose one consistently with its meandering observed in numerical experiments of Hwang and Cossu?[29] What is the physical mechanism driving the instability: a wake-type or a mixing layer type? Are the characteristic sizes of the unstable mode consistent with vortex clusters observed in the log-layer? With the aim of giving answers to these issues, we organize the paper as follows: in Sec. II, the stability theory for the organized motion and the numerical strategy will be shown. In Sec. III, after having briefly presented the idealized streaks associated with the log-layer, we will study their linear stability for three friction Reynolds numbers: $Re_\tau = 2000$, 3000, and 5000. After having discussed the relevance of a scenario that links vortex clusters to a streak instability in Sec. IV, Sec. V will be devoted to draw conclusions and perspectives.

II. GOVERNING EQUATIONS AND COMPUTATIONAL APPROACH

A. Equations of coherent motion and turbulent mean flow

Following Reynolds and Hussain,[24] the equations of organized waves are derived by introducing a so-called triple decomposition into the Navier-Stokes equations. A Newtonian eddy model is used to relate the Reynolds stress oscillation to the strain-rate of the fluctuations via an isotropic eddy viscosity. This crude modeling for the Reynolds stress can be questionable. Indeed, our study focuses on coherent motions that populate the intermediate region of a channel flow. In this log-law region, the Reynolds stresses are anisotropic (see the work of Pope[39] for a review). However, in the case of previous stability analyses devoted to the amplification of streaks in the logarithmic region of turbulent channel flows,[21,34] the influence of anisotropy is also neglected. In order to be consistent with the previous studies[21,34] devoted to the primary growth mechanism responsible for the formation of streaks in the log-layer, we use the same assumption. In the remainder of the paper, the instability of streaks will be analyzed.

Next, U_i and u_i represent the ith component of the turbulent mean flow ($\mathbf{U} = (U,V,W)^t$) and the coherent part of the velocity field ($\mathbf{u} = (u,v,w)^t$), respectively (i.e., $i = 1,2,3$ refer to the streamwise, wall-normal, and spanwise components, referenced hereafter as x, y, z). In a dimensionless form, u_i satisfy the following system:

$$\begin{cases} \dfrac{\partial u_i}{\partial t} + u_j \dfrac{\partial U_i}{\partial x_j} + U_j \dfrac{\partial u_i}{\partial x_j} + u_j \dfrac{\partial u_i}{\partial x_j} = -\dfrac{\partial p}{\partial x_i} + \dfrac{\partial}{\partial x_j}\left[\nu_T(y)\left(\dfrac{\partial u_i}{\partial x_j} + \dfrac{\partial u_j}{\partial x_i}\right)\right] \\ \dfrac{\partial u_i}{\partial x_i} = 0 \end{cases}, \tag{1}$$

where $\nu_T(y) = \nu(1 + \nu_t(y)/\nu)$ with ν the kinematic viscosity and $\nu_t(y)$ the turbulent eddy viscosity. Equations (1) are made dimensionless by using the friction velocity (u_τ) and the viscous length scale ($\delta_v = \nu/u_\tau$). For the total eddy viscosity, we use the semi-empirical expression initially proposed by Cess[40] for pipe flow. The total eddy viscosity is expressed in (2) and is built from a combination of van Driest's wall region law and Reichardt's middle law as reported by Reynolds and Tiederman[41] for channel flow,

$$\begin{cases} \nu_T(\eta) = \dfrac{1}{2}\left\{1 + \dfrac{k^2 Re_\tau^2}{9}(1-\eta^2)^2(1+2\eta^2)^2 \times \left(1 - \exp[|\eta| - 1]\dfrac{Re_\tau}{A}\right)\right\} + \dfrac{1}{2} \\ \eta = y/h \end{cases}, \tag{2}$$

with $Re_\tau = h/\delta_v$ the ratio between the half-width of the channel h and the viscous length scale δ_v. The constant k is the von Kármán constant and A is a constant characterizing the thickness of the wall region. The mean velocity profile is obtained by integrating $(1-\eta)u_\tau^2/\nu_T(\eta)$ along the wall normal direction. The authors del Alamo and Jiménez[21] fixed the two parameters A and k by least-square fitting the mean velocity profile recovered from DNS statistics of Hoyas and Jiménez.[42] The resulting values given by del Alamo and Jiménez,[21] $A = 25.4$ and $k = 0.424$, are used in this study. Next, data given in wall units (i.e., associated with δ_v and u_τ) are denoted with a + superscript (for instance,

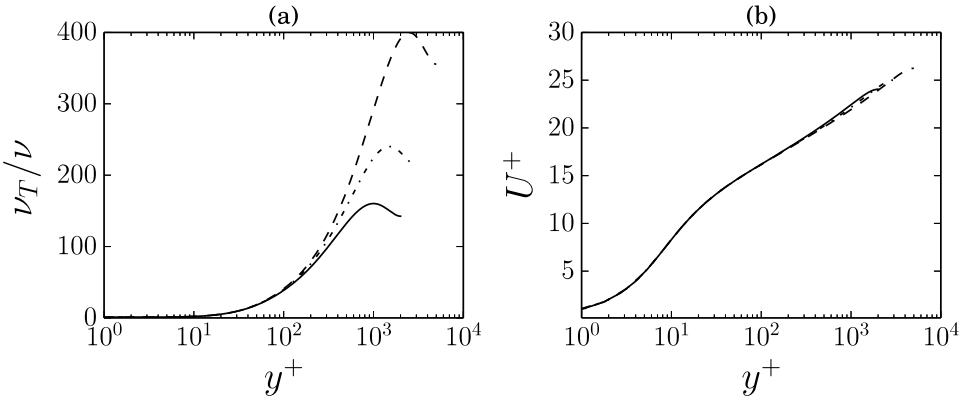

FIG. 1. (a) Cess eddy viscosity and (b) streamwise turbulent velocity profile plotted as a function of the distance normal to the wall scaled in wall units for $Re_\tau = 2000$ (——), 3000 (– – – –), and 5000 (- - - - - - - -).

$y^+ = y/\delta_v$ and $U^+ = U/u_\tau$). The eddy viscosity and turbulent streamwise velocity profiles are shown in Figures 1(a) and 1(b) for turbulent channel flows at $Re_\tau = 2000,\ 3000$, and 5000.

B. Nonlinear idealized saturated streaks

1. Optimal streamwise vortices

The nonlinear streaky base flow is computed from temporal evolution of the linear optimal initial condition in turbulent channels as proposed by Park *et al.*[38] for the outer region. For that purpose, system (1) is linearized about the turbulent mean velocity profile $U(y)$. Assuming wave-like organized motions, $\mathbf{u} = \hat{\mathbf{u}}(t)\, e^{i(\alpha x+\beta z)}$, system (1) can be recast as

$$\frac{\partial \hat{\mathbf{u}}}{\partial t} = \mathcal{L}\hat{\mathbf{u}}, \tag{3}$$

with α and β the streamwise and spanwise wavenumbers, respectively. Introducing the ratio of the kinetic energy associated with $\mathbf{u}$ to its kinetic energy at the initial time ($t = 0$), the optimal transient energy growth over all possible initial conditions is given by

$$G(\alpha,\beta,t) = \max_{\mathbf{u}(t=0)} \frac{\|\mathbf{u}\|}{\|\mathbf{u}_{(t=0)}\|}. \tag{4}$$

For shear flows, G reaches a maximum for $\alpha = 0$ (Ref. 20) at a given time $t = t_{\max}$. The corresponding initial condition takes the form of streamwise vortices that lead to infinitely elongated streaks at $t_{\max}$. In the analysis that follows, this initial condition is referred to as optimal streamwise vortices. The numerical method based on singular-value-decomposition of $e^{\mathcal{L}t}$ is detailed in the work of Alizard *et al.*[43]

2. Numerical simulation: Nonlinear development of streaks

Nonlinear system (1) is considered and the numerical solution is initialized by the optimal streamwise vortices. Fourier expansion is employed in the homogeneous direction z and Chebyshev polynomials are used in the wall-normal direction y. For time-stepping, a second order Adams-Bashforth is applied to the advective terms and a backward-differentiation scheme is used to advance the viscous terms. The Uzawa method is used for each Fourier mode to ensure that it is divergence-free (for more details, see Ref. 44). The truncated Fourier series are performed with the **DFFTPACK** library and a pseudospectral technique is used to evaluate the nonlinear terms. The "3/2" rule is implemented to remove the alias term. Once the nonlinear streak has reached a saturated amplitude, the linear stability of the secondary base flow is considered. One may also remark that the contribution of streamwise vortices is weak compared to a nonlinearly saturated streak when the latter reaches its maximum amplitude. For that purpose, we consider an equilibrium state $U_b(y,z)$ which satisfies

$$U_b(y,z) = U(y) + u_s(y,z) \tag{5}$$

with $u_s(y,z)$, the nonlinear saturated streak.

C. Secondary instability: Some theory

In accordance with Floquet theory for z-periodic equilibrium state, we consider the following normal solution associated with system (1) linearized about $U_b(y,z)$:

$$u_i(x,y,z,t) = e^{i\alpha x - \Omega t} \sum_{n=-\infty}^{\infty} \hat{u}_i(y)\, e^{i(n+\gamma)\beta z} + c.c, \tag{6}$$

where β is the spanwise wavenumber (i.e., associated with the streak spacing), α the streamwise wavenumber (i.e., associated with the streak instability), Ω the complex circular frequency, γ the detuning parameter, and $c.c$ the complex conjugate. Hereafter, we restrict our analysis to the fundamental mode, i.e., $\gamma = 0$. Introducing such a decomposition into system (1) and linearizing around U_b, one obtains the eigenproblem

$$(\mathcal{A} - i\Omega\mathcal{B})\,\widetilde{\mathbf{q}} = 0, \tag{7}$$

with $\widetilde{\mathbf{q}}(y,z) = (\widetilde{u},\widetilde{v},\widetilde{w})^t(y,z) = \sum_{n=-N}^{N} (\hat{u},\hat{v},\hat{w})^t(y)\, e^{in\beta z}$, where $2N+1$ refers to the number of Fourier modes. For a given mode, the real and imaginary parts of the eigenvalue Ω (referenced as Ω_r and Ω_i hereafter) represent the circular frequency and the temporal amplification rate, respectively. In particular, the corresponding mode is temporally amplified when Ω_i is positive and its phase speed is given by Ω_r/α. Eigenvalue problem (7) is discretized with the same spatial discretization as the one used for the numerical simulation. The implicitly restarted Arnoldi algorithm from the **ARPACK** library[45] is then used to solve (7). Note that the most amplified mode may also be studied through integration in time of (1) by replacing $\partial/\partial x$ with $i\alpha$.

After a grid sensitivity analysis, we only present the results obtained with the finest grid having 200 collocation points in the wall-normal direction and 48 Fourier modes for the spanwise direction. For instance, computations using 150 collocations points and 32 Fourier modes exhibit a difference of less than 0.5% for the characteristic temporal and spatial scales shown in this study.

Finally, for the stability analysis, problem (7) can be decoupled into even and odd modes with respect to the low speed streak symmetry plane, corresponding to $z = 0$ here (also called sinuous and varicose modes, respectively). In the case of even-symmetry (sinuous type),

$$\begin{gathered} u(x,y,z,t) = -u(x,y,-z,t),\ v(x,y,z,t) = -v(x,y,-z,t) \\ \text{and } w(x,y,z,t) = w(x,y,-z,t), \end{gathered} \tag{8}$$

while for the case of odd-symmetry (varicose type),

$$\begin{gathered} u(x,y,z,t) = u(x,y,-z,t),\ v(x,y,z,t) = v(x,y,-z,t) \\ \text{and } w(x,y,z,t) = -w(x,y,-z,t). \end{gathered} \tag{9}$$

Setting the odd- or even-symmetry results in reducing the storage requirement. The validation of the numerical methods is discussed in the Appendix.

III. SECONDARY INSTABILITY IN THE LOG-LAYER

A. Neutral log-layer modes

To quantify a possible secondary instability that may occur in the log-layer, we first discuss normal mode solutions of system (7) over a range of streak amplitudes. Following Park *et al.*,[38] the nonlinear evolution of streaks is computed by integrating in time the optimal streamwise vortices with an initial amplitude defined as

$$A_v = \left(\frac{2}{h\lambda_z} \int_0^h \int_{-\lambda_z/2}^{\lambda_z/2} u^2 + v^2 + w^2 \mathrm{d}y\mathrm{d}z \right)^{1/2}. \tag{10}$$

The streak amplitude is expressed as

$$A_s = \frac{\max_{y,z} u_s(y,z) - \min_{y,z} u_s(y,z)}{2U_c}, \tag{11}$$

where U_c represents the maximum mean streamwise velocity. For a given Reynolds number, the threshold values for a neutral growth rate are denoted with a cr subscript. The corresponding modes are hereafter referred to as neutral modes.

In the following, characteristic length scales of the organized motion associated with secondary instability are supposed to be fixed by the neutral mode. It means that we assume that threshold amplitudes for streak breakdown are close to $(A_s)_{cr}$ and that the time required to trigger the streak breakdown is short compared to its decay. Hence, the streamwise size of coherent motion is estimated by $\lambda_x = 2\pi/\alpha_{cr}$ for a given spanwise extent $\lambda_z = 2\pi/\beta$.

Finally, to characterize the vertical size of neutral modes, we also define a typical length scale (Λ_y) as the wall distance at which the cumulative modal kinetic energy is 80% of the total, i.e.,

$$\int_{-\lambda_z/2}^{\lambda_z/2}\int_0^{\Lambda_y}(u^2+v^2+w^2)\mathrm{d}\varepsilon\mathrm{d}\eta = 0.8\int_{-\lambda_z/2}^{\lambda_z/2}\int_0^{h}(u^2+v^2+w^2)\mathrm{d}\varepsilon\mathrm{d}\eta. \tag{12}$$

The procedure is here briefly outlined. For a given β, we compute the optimal streamwise vortices that lead to infinitely elongated streaks reaching a maximum transient energy growth in time. Then, the nonlinear evolution of streamwise streaks is generated by integrating (1) initialized with initial vortices of amplitude A_v. The neutral amplitude $(A_s)_{cr}$ is thus the lowest streak amplitude for which the maximum growth rate of the streak instability mode over α is zero.

For instance, effects of nonlinearity on the time evolution of streaks for different initial vortex amplitudes are displayed in Figure 2(a) for $\lambda_z^+ = 2244$ and $Re_\tau = 5000$. In Figure 2(b), a typical nonlinear saturated streak is illustrated by its streamwise velocity in the cross-stream (y^+, z^+) plane extracted at the time at which the corresponding amplitude A_s is maximum (referenced as $(A_s)_{\max}$). As observed in the laminar case by Anderson *et al.*,[46] the low-speed streak is displaced further away from the wall due to nonlinearities. It leads to the formation of regions of strong spanwise shear on both sides of the low-speed streak. For this case, we find that the mode associated with the highest temporal growth rate is sinuous. In particular, Figure 3(a) shows that the saturated low-speed streak becomes unstable when its amplitude exceeds 18% of the maximum mean velocity. The critical parameters $(\alpha_{cr}^+, (A_s)_{cr})$ associated with a neutral growth rate are shown in Figure 3(b).

Neutral modes are then computed for several $\lambda_z^+ = (2\pi/\beta)/\delta_v$ wider than $100\delta_v$ (i.e., corresponding to larger structures than those of the buffer layer). The neutral modes are sinuous for all λ_z^+ considered (i.e., varicose modes are found to be temporally damped) consistent with Hwang and Cossu.[29] Phase speeds of neutral modes ($c^+ = (\Omega_r/\alpha_{cr})/u_\tau$) are shown as a function of the

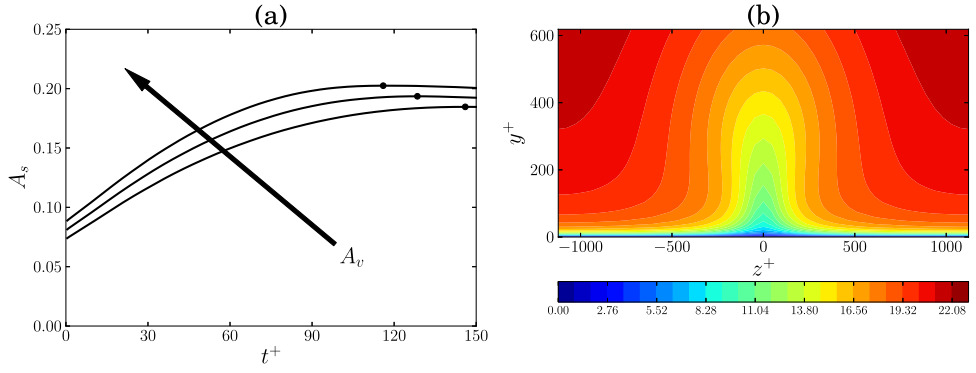

FIG. 2. Base flow simulations at $Re_\tau = 5000$ and $\lambda_z^+ = 2244$. (a) Streak amplitudes *vs* time scaled in wall units for three initial amplitudes of optimal streamwise vortices $A_v = 0.05,\ 0.055$, and 0.06. The maximum amplitude, $(A_s)_{\max}$, is denoted by •. (b) Streamwise velocity contours in wall units of the nonlinear saturated low-speed streak for the time indicated by • in (a) and $A_v = 0.05$.

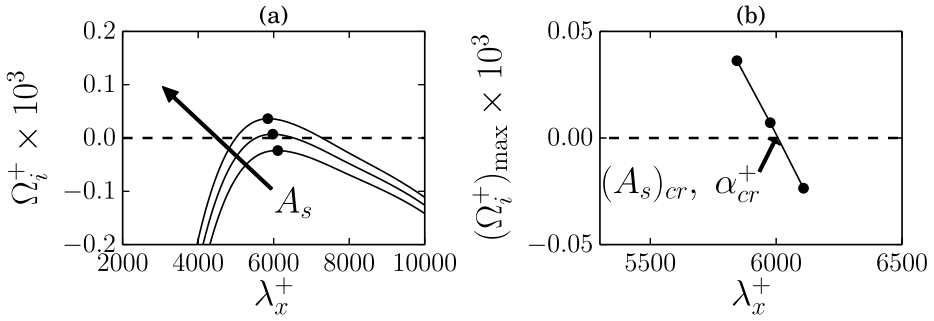

FIG. 3. Secondary instability analysis performed at $Re_\tau = 5000$ and $\lambda_z^+ = 2244$. (a) The temporal growth rate of the most amplified mode *vs.* the streamwise wavelength $\lambda_x^+ = (2\pi/\alpha)/\delta_v$ is shown for $(A_s)_{\max} = 0.185,\ 0.186$, and 0.188. The maximum value of the temporal growth rate, $(\Omega_i^+)_{\max}$, is denoted by •. (b) The distribution of $(\Omega_i^+)_{\max}$ with the streamwise wavelength λ_x^+. The critical parameters (i.e., associated with a neutral temporal growth rate) are also indicated with the subscript cr.

vertical length scale Λ_y^+ in Figure 4 for $Re_\tau = 5000$ and for λ_z^+ ranging from 1420 to 3500. The mean streamwise velocity profile is also represented. Figure 4 shows that flow structures associated with neutral modes propagate downstream with a speed close to the local mean velocity associated with the logarithmic region. As a consequence, we may classify these modes as neutral log-layer modes. In particular, the latter behavior is consistent with the Taylor's frozen-turbulence hypothesis.[47] One may remark that this feature has also been observed by Moarref *et al.*[35] for optimal modes corresponding to streaks localized in the logarithmic region. Figure 5 shows streamwise, wall-normal, and spanwise velocity components of the neutral log-layer mode for $\lambda_z^+ = 2244$, $(A_s)_{cr} \approx 18\%$, $\lambda_x^+ = 2\pi/\alpha_{cr}^+ \approx 6000$, and $Re_\tau = 5000$. The critical layer, i.e., the line where the mean velocity is equal to the phase speed c^+, is also reported. It shows that regions associated with maximum amplitudes of velocity components are concentrated near the critical layer. This observation further provides strong evidence for the importance of the critical layer in triggering secondary instability.

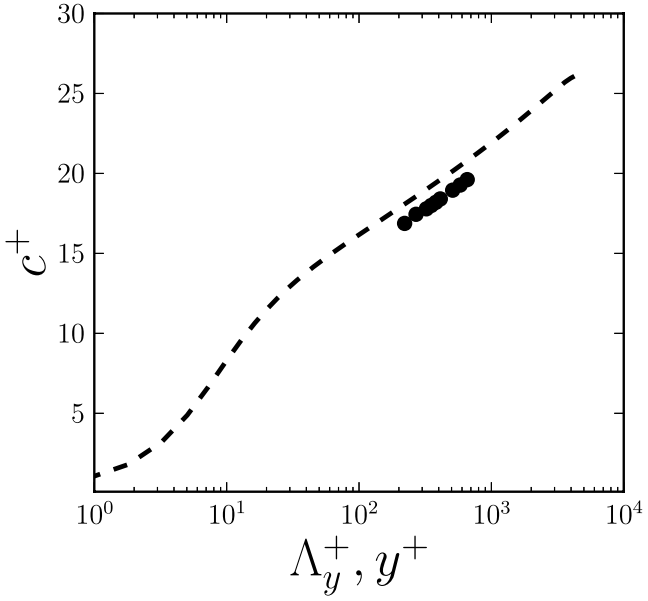

FIG. 4. Neutral log-layer modes for $Re_\tau = 5000$ and λ_z^+ ranging from 1420 to 3500 (•): the phase speed in the streamwise direction c^+ is shown as a function of the vertical length scale Λ_y^+. The dashed line represents the mean streamwise velocity as a function of the wall-normal direction y^+.

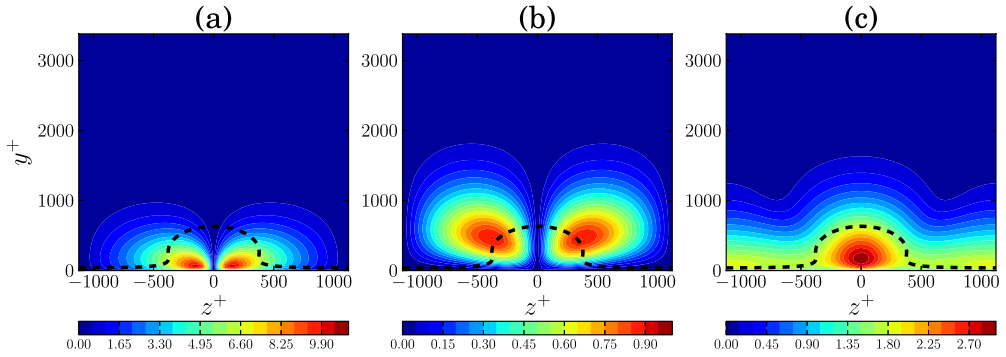

FIG. 5. Cross-stream ($y^+ - z^+$ plane) view of the eigenfunctions associated with the neutral log-layer mode for $Re_\tau = 5000$, $\lambda_z^+ = 2244$, and $\lambda_x^+ = 6000$. (a) $|u|$, (b) $|v|$, and (c) $|w|$. The position of the critical layer is also shown in dashed lines.

B. Geometrical self-similarity of neutral log-layer modes

Based on numerical experiments, del Alamo *et al.*[31] and Hwang and Cossu[29] show that organized structures populating the logarithmic layer exhibit a geometric self-similarity, namely, their wall-parallel length scales vary linearly with the distance from the wall. In particular, the previous authors show that coherent motions are self-sustained and the process involves the streak breakdown and regeneration of streamwise vortices. Assuming that there is a correspondence between the streak breakdown and modal secondary instability, the self-similar growth of neutral log-layer modes is investigated for Re_τ = 2000, 3000, and 5000. From Sec. III A, we consider hereafter a characteristic length for the wall-normal direction based on the critical layer position such as

$$y_c^+ = \max_{z^+} \left(y^+ \mid U_b\left(y^+, z^+\right) = c^+ \right). \tag{13}$$

In Figure 6(a), we report the distribution of both the streamwise and spanwise sizes (i.e., $\lambda_x^+ = (2\pi/\alpha_{cr})/\delta_v$ and $\lambda_z^+ = (2\pi/\beta)/\delta_v$, respectively) as a function of the wall distance y_c^+. It is observed that both characteristic spanwise and streamwise lengths associated with neutral log-layer modes depend linearly on y_c^+. Figure 6(a) also shows that $\lambda_z^+(y_c^+)$ and $\lambda_x^+(y_c^+)$ fall on a nearly universal curve. These results are in agreement with simulations of Hwang and Cossu[29] who have verified that organized sinuous streaky motions exhibit a universal behavior in the logarithmic region independently of the Reynolds number. In particular, in our analysis, we found that $\lambda_z^+ \approx 3.3 y_c^+$ and $\lambda_x^+ \approx 10 y_c^+$.

Attached coherent structures are observed to grow self-similarly with time by del Alamo *et al.*[31] As noted by Moarref *et al.*,[35] a representative time scale can be defined as $t^+ = \lambda_x^+/c^+$ where t^+

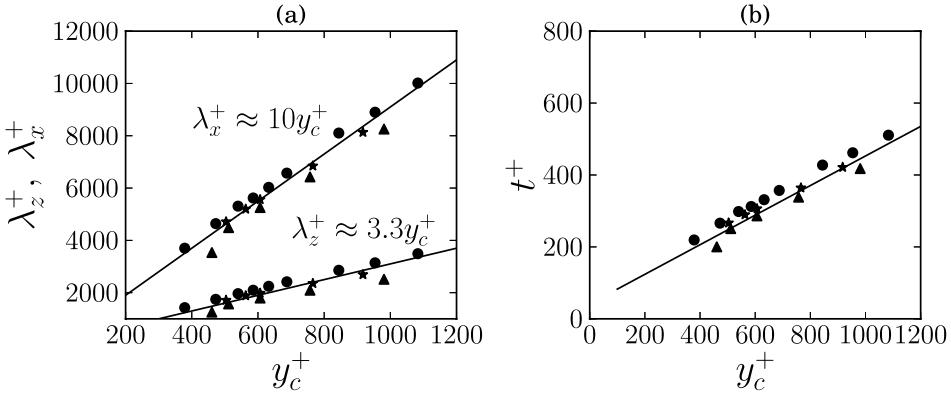

FIG. 6. Neutral log-layer modes: (a) spanwise and streamwise wavelengths and (b) convective time scale $t^+ = \lambda_x^+/c^+$ reported as a function of the distance from the wall y_c^+ for flow cases $Re_\tau = 2000,\ 3000$, and 5000 (▲, ★, and ●, respectively).

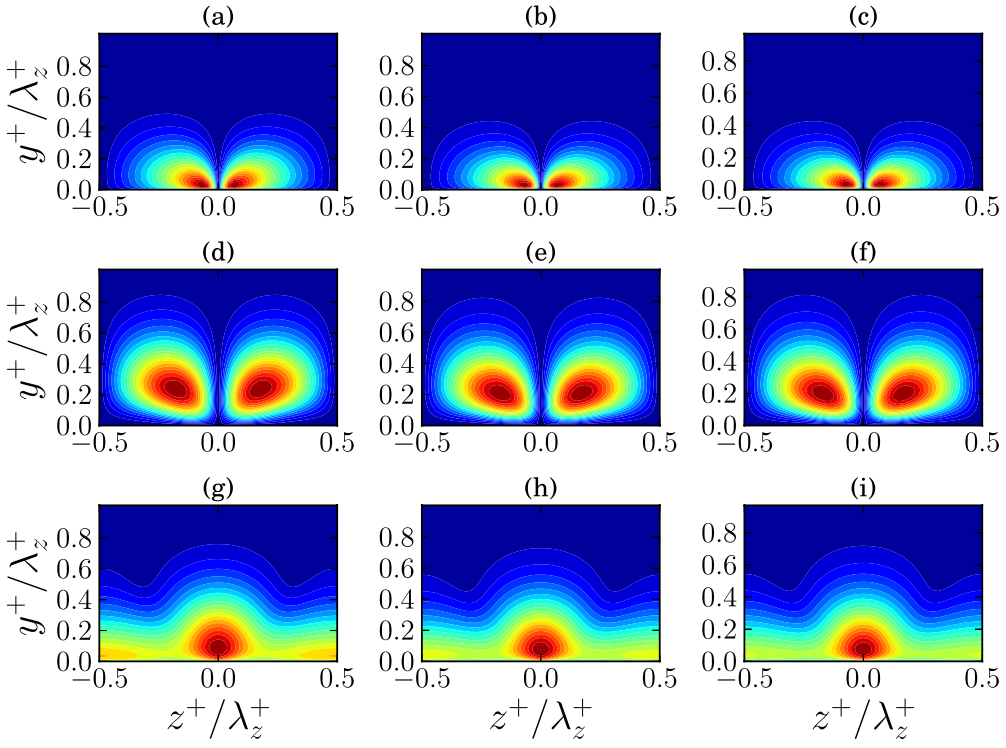

FIG. 7. Neutral log-layer modes for $Re_\tau = 5000$: cross-stream ($y^+/\lambda_z^+ - z^+/\lambda_z^+$ plane) view of the eigenfunctions for $\lambda_z^+ = 3490$ ((a), (d), (g)), $\lambda_z^+ = 2244$ ((b), (e), (h)), and $\lambda_z^+ = 1745$ ((c), (f), (i)). The normalized amplitudes of the streamwise, wall-normal, and spanwise components of the modes are shown in ((a), (b), (c)), ((d), (e), (f)), and ((g), (h), (i)), respectively. Same contour levels as in Figure 5. The contours are plotted in coordinates scaled by λ_z^+ to account for geometrical similarity.

represents the time over which the wave associated with the neutral log-layer mode convects downstream for one wavelength. In Figure 6(b), the distribution of t^+ as a function of the distance from the wall y_c^+ is reported. The figure shows that the size of such a mode will increase linearly with time, in agreement with the numerical experiments of del Alamo *et al.*[31] In addition, this behavior is independent of Re_τ when using an inner scaling. The observed time self-similar evolution also agrees with a universal behavior for secondary modes in the logarithmic region.

Figure 6(a) suggests that neutral log-layer modes are geometrically self-similar. To confirm this behavior, we plot in Figure 7 the eigenfunctions associated with neutral log-layer modes in similarity variables: y^+/λ_z^+ and z^+/λ_z^+, for three representative spanwise wavelengths: $\lambda_z^+ = 1745$, 2244, and 3490, and $Re_\tau = 5000$. The rescaled shapes are seen to be nearly independent of λ_z^+. It further supports that neutral log-layer modes are geometrically self-similar and are thus compatible with the concept of attached eddies proposed by Townsend.[6]

C. Streak instability mechanism

1. *Kinetic energy budget*

For having a physical understanding of the stabilizing effect of streaks on the Tollmien-Schlichting instability in the laminar boundary layer, Cossu and Brandt[48] used the equation associated with the perturbation kinetic energy. Here, we extend this framework to turbulent flows. The basic idea is to derive the evolution equation for the kinetic energy associated with the organized motion from the linearized version of system (1). We denote E the spatial integration of the kinetic energy density: $e = (uu^\star + vv^\star + ww^\star)$ where * stands for the complex conjugate,

$$E = \int_{-\lambda_z/2}^{\lambda_z/2} \int_0^h uu^\star + vv^\star + ww^\star \mathrm{d}z\mathrm{d}y. \tag{14}$$

Therefore, the temporal evolution of E is rewritten as

$$\frac{\partial E}{\partial t} = T_{uy} + T_{uz} - D_m - D_t, \tag{15}$$

where the terms on the right hand side are defined as

$$T_{uy} = -\int_{-\lambda_z/2}^{\lambda_z/2}\int_0^h \left(u^\star v + u v^\star\right)\frac{\partial U_b}{\partial y}\mathrm{d}z\mathrm{d}y, \tag{16}$$

$$T_{uz} = -\int_{-\lambda_z/2}^{\lambda_z/2}\int_0^h \left(u^\star w + u w^\star\right)\frac{\partial U_b}{\partial z}\mathrm{d}z\mathrm{d}y, \tag{17}$$

$$\begin{aligned} D_m = \frac{1}{Re_\tau}\int_{-\lambda_z/2}^{\lambda_z/2}\int_0^h &\left(\frac{\partial^2 u}{\partial y^2} + \frac{\partial^2 u}{\partial z^2} - \alpha^2 u\right)u^\star + \left(\frac{\partial^2 u^\star}{\partial y^2} + \frac{\partial^2 u^\star}{\partial z^2} - \alpha^2 u^\star\right)u + \\ &\left(\frac{\partial^2 v}{\partial y^2} + \frac{\partial^2 v}{\partial z^2} - \alpha^2 v\right)v^\star + \left(\frac{\partial^2 v^\star}{\partial y^2} + \frac{\partial^2 v^\star}{\partial z^2} - \alpha^2 v^\star\right)v + \\ &\left(\frac{\partial^2 w}{\partial y^2} + \frac{\partial^2 w}{\partial z^2} - \alpha^2 w\right)w^\star + \left(\frac{\partial^2 w^\star}{\partial y^2} + \frac{\partial^2 w^\star}{\partial z^2} - \alpha^2 w^\star\right)w\mathrm{d}z\mathrm{d}y, \end{aligned} \tag{18}$$

and

$$\begin{aligned} D_t = \frac{1}{Re_\tau}\int_{-\lambda_z/2}^{\lambda_z/2}\int_0^h &\nu_t\left(\frac{\partial^2 u}{\partial y^2} + \frac{\partial^2 u}{\partial z^2} - \alpha^2 u\right)u^\star + \nu_t\left(\frac{\partial^2 u^\star}{\partial y^2} + \frac{\partial^2 u^\star}{\partial z^2} - \alpha^2 u^\star\right)u + \\ &\nu_t\left(\frac{\partial^2 v}{\partial y^2} + \frac{\partial^2 v}{\partial z^2} - \alpha^2 v\right)v^\star + \nu_t\left(\frac{\partial^2 v^\star}{\partial y^2} + \frac{\partial^2 v^\star}{\partial z^2} - \alpha^2 v^\star\right)v + \\ &\nu_t\left(\frac{\partial^2 w}{\partial y^2} + \frac{\partial^2 w}{\partial z^2} - \alpha^2 w\right)w^\star + \nu_t\left(\frac{\partial^2 w^\star}{\partial y^2} + \frac{\partial^2 w^\star}{\partial z^2} - \alpha^2 w^\star\right)w + \\ &\frac{d\nu_t}{dy}\left(\frac{\partial u}{\partial y} + i\alpha v\right)u^\star + \frac{d\nu_t}{dy}\left(\frac{\partial u^\star}{\partial y} + i\alpha v^\star\right)u + \\ &2\frac{d\nu_t}{dy}v^\star\frac{\partial v}{\partial y} + 2\frac{d\nu_t}{dy}v\frac{\partial v^\star}{\partial y} + \frac{d\nu_t}{dy}\left(\frac{\partial w^\star}{\partial y} + \frac{\partial v^\star}{\partial z}\right)w + \frac{d\nu_t}{dy}\left(\frac{\partial w}{\partial y} + \frac{\partial v}{\partial z}\right)w^\star\mathrm{d}z\mathrm{d}y. \end{aligned} \tag{19}$$

The quantity E is the total perturbation kinetic energy, D_m is the viscous dissipation term, and T_{uy} and T_{uz} are the production terms associated with the work of the Reynolds stresses against the wall-normal shear and spanwise shear of the mean flow, $\partial U_b/\partial y$ and $\partial U_b/\partial z$, respectively. Equation (15) incorporates also the contribution of disorganized smaller scales through the dissipation term D_t. Under a normal mode hypothesis, the terms in the energy balance equation can be recast into

$$\left(E, D_m, D_t, T_{uy}, T_{uz}\right) = \left(\hat{E}, \hat{D_m}, \hat{D_t}, \hat{T_{uy}}, \hat{T_{uz}}\right)e^{2\Omega_i t}. \tag{20}$$

The temporal amplification rate of a given mode is then derived from

$$\Omega_i = \frac{\hat{T_{uy}}}{2\hat{E}} + \frac{\hat{T_{uz}}}{2\hat{E}} - \frac{\hat{D_m}}{2\hat{E}} - \frac{\hat{D_t}}{2\hat{E}}. \tag{21}$$

When focusing on neutral modes, the total dissipation and the work of the Reynolds stresses against the wall-normal shear and spanwise shear are balanced. Equation (21) reduces to

$$T_{uy} + T_{uz} = D_m + D_t. \tag{22}$$

In Figure 8, we report the different terms entering Equation (22) for the neutral log-layer mode associated with $\lambda_z^+ = 2244$ and $Re_\tau = 5000$, for illustration purposes. The figure shows that the secondary instability is ascribed to the excess of kinetic energy production term associated with the Reynolds stress against the mean spanwise shear (T_{uz}) over the dissipation. A dominating contribution of the dissipation due to smaller scales over the molecular one is observed as expected in the log-layer. Similar results are obtained for all neutral log-layer modes shown in Figure 6. From the above discussion, we may approximate Equation (22) with $T_{uz} \approx D_t$, in the logarithmic region. This suggests that the dominant sinuous log-layer mode can occur mainly through the spanwise shear. In Figure 9, T_{uz} is

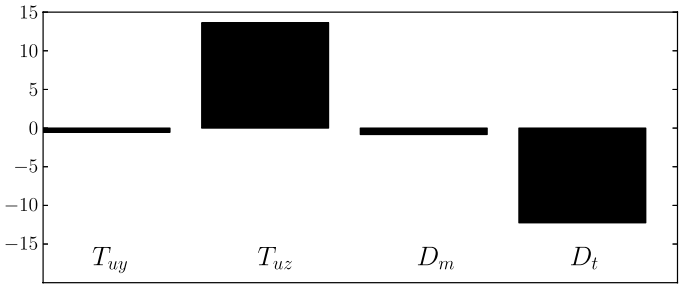

FIG. 8. Neutral log-layer modes: Production and dissipation terms of disturbance kinetic energy for $\lambda_z^+ = 2244$ and $Re_\tau = 5000$.

displayed as a function of the distance from the wall y_c^+ for $Re_\tau = 2000,\ 3000$, and 5000. This shows that the kinetic energy production term is inversely proportional to y_c^+ such as

$$\log\left(T_{uz}\right)\left(y_c^+\right) = A - \log\left(y_c^+\right), \tag{23}$$

with A a constant that depends of Re_τ. This, thus, gives strong evidence that a universal mechanism is at the origin of the triggering of streak instability for modes populating the logarithmic region, consistent with Townsend.[6] Figure 9 also shows that production term T_{uz} increases with the Reynolds number. Using the energy balance equation $T_{uz} \approx D_t$, Figure 9 shows that the amount of dissipation due to the disorganized smaller scales increases with the Reynolds number in order to prevent an unlimited growth of turbulence. Finally, one may observe in Figure 9 that, as the distance from the wall increases, less energy extracted from the mean flow is necessary to overcome the dissipation due to smaller scales.

2. *Vorticity perturbation components*

Schoppa and Hussain[27] address an analogy between the dominant sinuous mode of the buffer-layer (hereafter referred to as buffer-layer mode) and a three-dimensional instability of a planar mixing layer. To further examine if the instability mechanism associated with neutral log-layer modes bears close resemblance to the one identified by Schoppa and Hussain,[27] a projection of the perturbation vorticity components onto a local coordinate system associated with iso-contours of U_b is considered

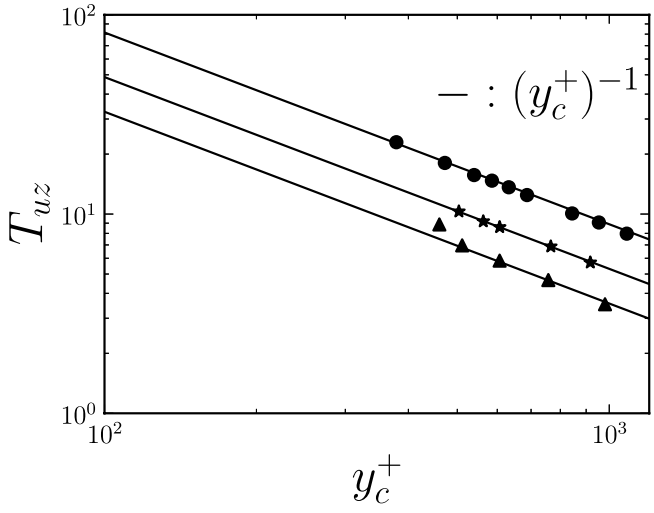

FIG. 9. Neutral log-layer modes: distribution of the production term T_{uz} associated with the work of the Reynolds stress against the spanwise shear as a function of the distance from the wall y_c^+ for $Re_\tau = 2000,\ 3000$, and 5000 (▲, ⋆, and ●, respectively).

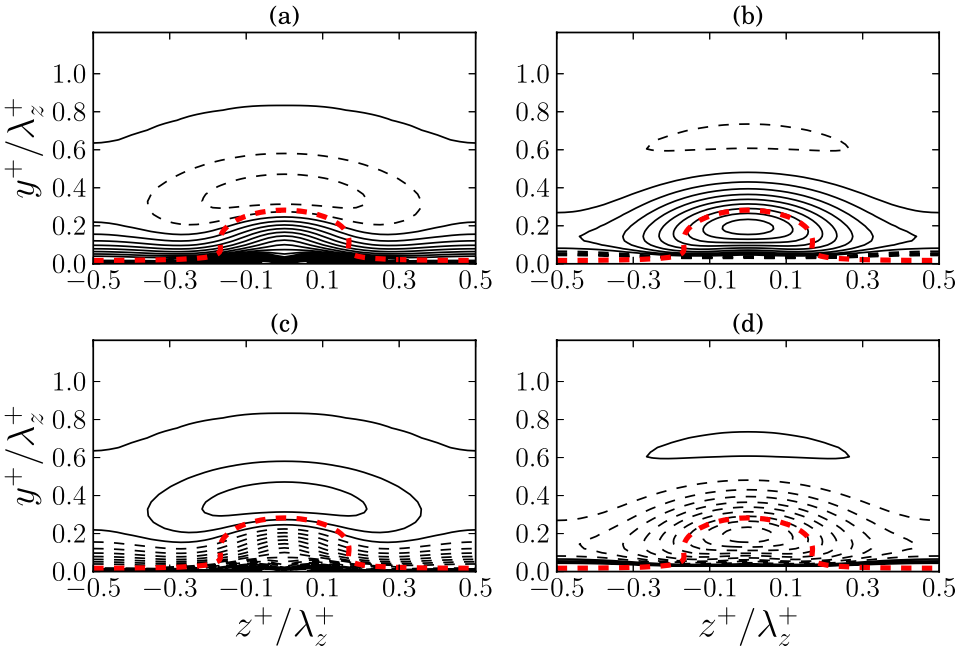

FIG. 10. The streamwise vorticity component associated with the neutral log-layer mode for $Re_\tau = 5000$ and $\lambda_z^+ = 2244$ at (a) $\alpha x = 0$, (b) $\alpha x = \pi/2$, (c) $\alpha x = \pi$, and (d) $\alpha x = 3\pi/2$. Solid (dashed) lines represent positive (negative) contours. The critical layer position is shown in red thick dashed lines.

hereafter. The wall-normal (ω_y) and spanwise (ω_z) vorticity components are thus transformed as

$$\begin{cases} \omega_s = \omega_y \dfrac{\partial U_b}{\partial z}\dfrac{1}{N} - \omega_z \dfrac{\partial U_b}{\partial y}\dfrac{1}{N} \\ \omega_n = \omega_y \dfrac{\partial U_b}{\partial y}\dfrac{1}{N} + \omega_z \dfrac{\partial U_b}{\partial z}\dfrac{1}{N} \\ \text{with } N = \sqrt{\left|\dfrac{\partial U_b}{\partial y}\right|^2 + \left|\dfrac{\partial U_b}{\partial z}\right|^2} \end{cases}, \tag{24}$$

where tangential and normal coordinates with respect to base flow vortex lines are denoted as s and n, respectively. The streamwise vorticity component (ω_x) is not modified. As observed by Schoppa and Hussain[27] for the buffer-layer mode, Figures 10–12 show that the streak instability mechanism is fully three-dimensional. As the U_b contour bends up, the streamwise vorticity is tilted along the crest of the low-speed streak and forms a dipole-like structure. The critical layer separates curved sheets of ω_x of opposite signs that induce positive and negative spanwise velocities near the crest of the low-speed streak. Hence, similarly to the buffer layer mode, the sinuous motion driven by the streak instability is mainly caused by the ω_x distribution. As shown in Figure 11, the tangential vorticity component is mainly located on the flanks of the low-speed streak (i.e., regions of strongest spanwise shear), where the critical layer separates positive and negative values of ω_s. This vorticity component will force the curved-sheets to roll-up along the critical layer into a spiral form. The latter mechanism closely resembles the shear-layer instability of a z-periodic mixing-layer associated with the buffer-layer mode as described by Schoppa and Hussain.[27]

Finally, in Figure 12, we show that opposite-signed ω_n contours overlap on both sides of the low speed streak near the critical layer. As underlined by Schoppa and Hussain,[27] these overlap regions are also observed for the buffer-layer mode but not for three-dimensional instability modes associated with a mixing layer. This minor normal vorticity difference excepted, the streak instability associated with neutral log-layer mode is seen to involve the same instability mechanism as mixing layer oblique modes. It also exhibits strong similarities with the streak instability mechanism described by Schoppa and Hussain[27] for the buffer-layer mode.

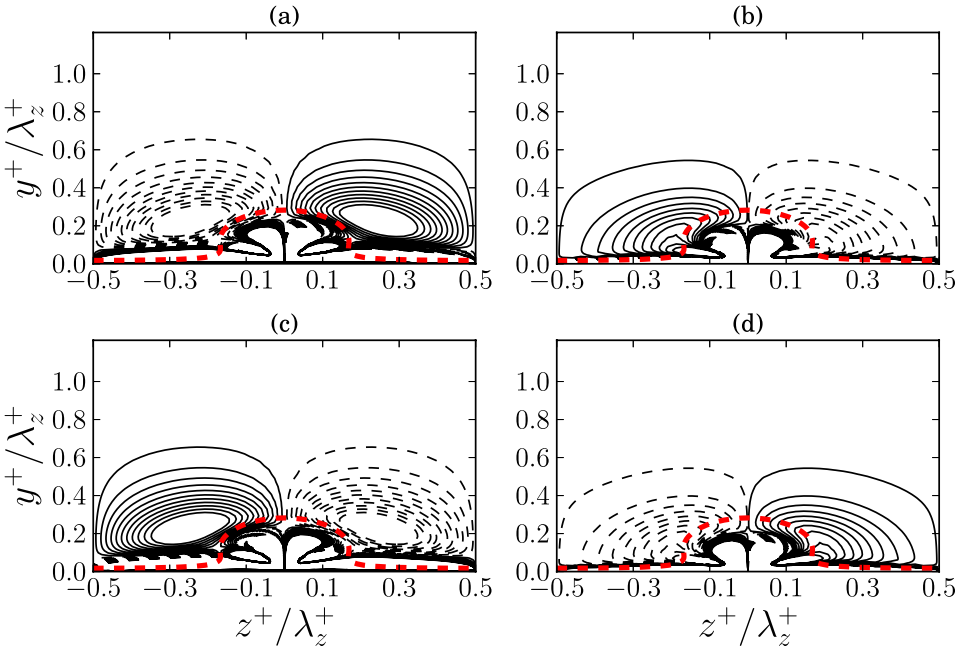

FIG. 11. The tangential vorticity component associated with the neutral log-layer mode for $Re_\tau = 5000$ and $\lambda_z^+ = 2244$ at (a) $\alpha x = 0$, (b) $\alpha x = \pi/2$, (c) $\alpha x = \pi$, and (d) $\alpha x = 3\pi/2$. Solid (dashed) lines represent positive (negative) contours. The critical layer position is shown in red thick dashed lines.

IV. DISCUSSION

As recently pointed out by Hwang,[30] self-sustaining attached eddies are composed of two distinct elements: a long streaky motion and a more compact vortical structure which is strongly three-dimensional. This second element may be associated with vortex clusters described by del

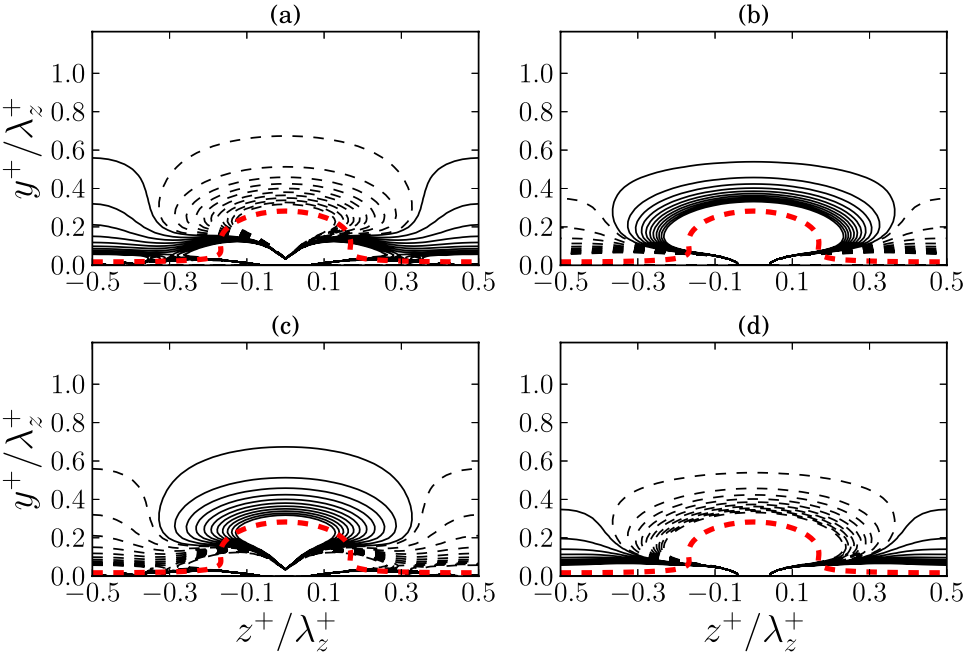

FIG. 12. The normal vorticity component associated with the critical log-layer mode for $Re_\tau = 5000$ and $\lambda_z^+ = 2244$ at (a) $\alpha x = 0$, (b) $\alpha x = \pi/2$, (c) $\alpha x = \pi$, and (d) $\alpha x = 3\pi/2$. Solid (dashed) lines represent positive (negative) contours. The critical layer position is shown in red thick dashed lines.

Alamo and Jiménez[21] that populate the log-layer. One-dimensional spectra extracted by Hwang[30] of isolated attached coherent motions associated with a given spanwise length scale exhibit also a bimodal behavior. In particular, Hwang[30] found that vortex clusters are self-similar along $y \approx 0.5\lambda_z \sim 0.7\lambda_z$ and $\lambda_x \approx 2\lambda_z \sim 3\lambda_z$. Using minimal flow simulations, del Alamo and Jiménez[21] have found that attached clusters are organized along $y \approx 0.3\lambda_z$ and $\lambda_x \approx 2\lambda_z$, where λ_z and λ_x represent the dimension of the boxes along the spanwise and streamwise directions, respectively, and y the distance from their centers to the wall. In our analysis, we have found that the size and the geometry of neutral log-layer modes roughly scale as

$$y \approx 0.3\lambda_z \quad \text{and} \quad \lambda_x \approx 3\lambda_z. \tag{25}$$

Scaling (25) appears consistent with those obtained from numerical experiments. Scaling (25) suggests that the vortex clusters identified by Hwang[30] and del Alamo and Jiménez[21] through numerical experiments could arise from an instability mechanism of the low-speed streak. The three-dimensional nature of the neutral log-layer mode also supports the increasing amount of energy associated with the spanwise velocity spectra observed by Hwang[30] for the vortex clusters.

A bimodal behavior is also observed in the outer-motion of turbulent boundary layers, channel flows, and pipe flows by Monty *et al.*[49] and Balakumar and Adrian,[50] for instance. In particular, for channel flows and pipe flows, the two-dominant modes of the energy spectra are classically identified as the **LSM** and the **VLSM**.[3] For channel flows, an energy peak emerges at $\lambda_x \approx 2h \sim 3h$ for $y > 0.3h$ in the spectra of all velocity components. This primary peak is associated with the **LSM** (see Monty *et al.*[49]). When focusing on the neutral log-layer mode with $\lambda_x = 3h$, we found $y \approx 0.3h$ and $\lambda_z = 1h$. This scaling is in agreement with characteristic sizes of **LSMs**. Hence, as expected, neutral log-layer modes populating the log-layer have characteristic sizes smaller than **LSMs** localized above the edge of the logarithmic region. Our analysis also supports the scenario conjecturing that **LSMs** are associated with quasi-streamwise vortices aligned to low-speed streaks (i.e., the **VLSMs**) and are caused by a streak instability (see Park *et al.*[38]).

However, as underlined by Schoppa and Hussain[27] for the buffer-layer mode, the linear growth of sinuous streak instability may itself not be sufficient to explain the regeneration of streaks. It may be supposed that disturbances associated with neutral log-layer modes will produce more representative streamwise vortices as they evolve into the nonlinear regime. Such a scenario could give further evidence about a wide range of autonomous self-sustained processes at intermediate scales associated with the logarithmic layer as recently suggested by Hwang and Cossu.[29]

Nevertheless, one might ask whether the modal instability of idealized streaks computed by using system (1) is able to predict the breakdown of streaks which are observed in direct numerical simulations. Trying to give a preliminary answer, we first introduce the parameter θ that characterizes the base-flow vortex line inclination angle for a given position in the plane (y^+, z^+),

$$\theta = \tan^{-1}\left(\frac{\partial U_b}{\partial z} \Big/ \frac{\partial U_b}{\partial y}\right). \tag{26}$$

We recall that base-flow vortex lines are defined as iso-contours of U_b; for more details, see Schoppa and Hussain.[27] The parameter θ is further illustrated in Figure 13. The "strength" of lifted streaks is thus described by the quantity θ_c such as

$$\theta_c = \max_{y^+, z^+}(\theta). \tag{27}$$

For neutral conditions (i.e., for $(A_s)_{cr}$ and α_{cr}), θ_c is plotted in Figure 14 as a function of the spanwise wavelength for $Re_\tau = 2000$, 3000, and 5000. When using a criterion based on θ_c, Figure 14 shows that the onset of a modal streak instability in the logarithmic region is nearly independent of the Reynolds number. In particular, θ_c is approximatively equal to 78° for all flow cases. Therefore, the sinuous mode associated with low-speed streaks becomes linearly unstable for relatively strong lifted angles. Schoppa and Hussain[27] found a streak lift angle $\theta_c \approx 50°$ for the onset of an instability mode for the streaks closest to the wall. One may remark that the value given by Schoppa and Hussain[27] has been estimated without adding an eddy viscosity in the stability equations. We have also performed a computation of secondary instability for streaks in the buffer region by using an eddy viscosity model (not shown here for the sake of conciseness). The "strength" of lifted streaks for neutral conditions

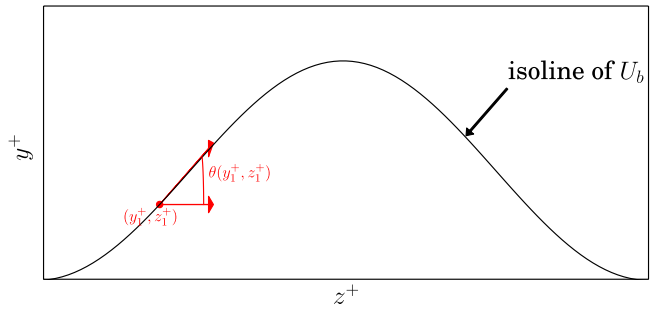

FIG. 13. Illustration of the base-flow vortex line inclination angle θ for a given position (y_1^+, z_1^+) localized on an isoline of U_b.

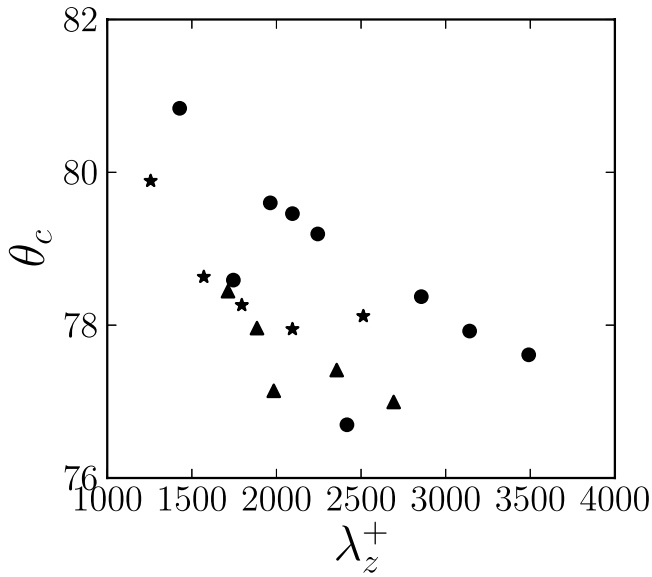

FIG. 14. Neutral log-layer mode: distribution of the maximum streak lift angle as a function of the spanwise wavelength scaled in inner units for $Re_\tau = 2000$, 3000, and 5000 (▲, ⋆, and •, respectively).

is found to be $\theta_c \approx 78°$ which is consistent with the threshold obtained for neutral log-layer modes. Addressing streak instability in the buffer region and considering the large value obtained for θ_c, Schoppa and Hussain[27] give further argument for a secondary transient growth scenario for streaks closest to the wall. As a consequence, one may ask if perturbations of linearly stable low-speed streaks in the log-layer may also experience a transient energy growth and then trigger nonlinear mechanism that will lead to the breakdown of streaks. Recently, Jiménez[26] proposes such a scenario by analyzing the burst of coherent structures of the logarithmic layer in turbulent channel flows in "minimal" computational boxes. In particular, Jiménez[26] argues that an Orr mechanism[51] is the way in which instabilities of streaks grow.

V. CONCLUSION AND OUTLOOKS

The secondary instability of turbulent channel flow streaks that populate the log-layer has been investigated for three Reynolds numbers. By using the system of equations developed by Park *et al.*,[38] we showed that nonlinear low-speed streaks localized in the logarithmic region may experience a modal instability. In particular, a sinuous mode is seen to be unstable for a low-speed streak strength $\theta_c \approx 78°$, independently of the Reynolds number. For the modal instability threshold, the speed of the neutral log-layer mode equals the local turbulent mean velocity, giving some evidence about the

influence of the critical layer onto the onset of the instability. In addition, neutral log-layer modes exhibit a geometrically self-similar behavior. Moreover, both the spanwise and streamwise sizes of neutral log-layer modes appear to be proportional to their distance from the wall, which is in agreement with the concept of attached eddies developed by Townsend.[6] Furthermore, these modes are found to be self-similar along $y \approx 0.3\lambda_z$ and $\lambda_x \approx 3\lambda_z$ in agreement with the numerical experiments of del Alamo *et al.*[31] and Hwang.[30]

Finally, an analysis of the vorticity components of neutral log-layer modes suggests that the vortex clusters can be triggered by the roll-up of vorticity at the edge of a low-speed streak, similarly to a three-dimensional mixing layer. In particular, this mechanism has many similarities to the one associated with the buffer-layer as described by Schoppa and Hussain.[27] The latter remark is also consistent with the observation of Pirozzoli and Bernardini[52] who suggest a similar mechanism for the creation of vortex tubes from streaks, near the wall of turbulent boundary layers.

Based on these results, one may propose that the second element of an attached eddy (i.e., the quasi-streamwise vortices) originates from a secondary instability. While the present study supports the self-sustaining nature of attached eddies in the logarithmic region, it also gives some further insight about the underlying instability mechanism. In addition, the streamwise vorticity distribution of the log-layer instability mode also suggests a streaks regeneration mechanism.

Despite these encouraging results, the onset of a modal instability is only observed for strongly lifted streaks. This behaviour may thus give some arguments for a scenario based on secondary transient growth. For a laminar boundary layer flow, Hoepffner *et al.*[53] show that perturbations of streaks can grow in a short-time scale due to the tilting of initial disturbances into the direction of the mean shear, similarly to what it is observed for the Orr-mechanism. For subcritical conditions, Hoepffner *et al.*[53] also show that such a perturbation could transiently reach a high level of energy. Cossu and Henningson[54] computed the optimal growth of perturbations to transiently growing streaks in a laminar Poiseuille flow. They observed that a secondary transient energy growth exhibits a similar mechanism of the primary growth of streaks. In particular, for subcritical conditions, the linear analysis fails to ascribe the streaks breakdown to a secondary transient growth mechanism. However, Cossu *et al.*[55] performed nonlinear stability of laminar sinuous lifted streaks for the plane Couette flow. The amplitude for the breakdown of nonlinear saturated streaks is observed to decrease when considering the scenario of secondary transient energy growth. This analysis gives some argument about a bypass scenario for the streak breakdown well below the onset of an unstable mode when considering the influence on nonlinearities. Such theories are currently under investigation. Finally, to evaluate the relevance of the linear theory for streak instability, Hack and Zaki[56] carried out statistical evaluations of the magnitude of streaks that populate a laminar boundary layer and compared these results with the threshold given by the modal stability analysis. Hence, the extension of this analysis to a turbulent channel flow could be an interesting perspective.

Furthermore, we may also draw some criticism concerning the considered base flow. In particular, as noticed by Vaughan and Zaki[57] in a laminar regime, the secondary instability threshold is altered by the choice of the streaky base flow. This could be also suggested for turbulent flows. Nevertheless, a robust numerical procedure to extract relevant streaks in turbulent flows remains an open question. Addressing wall-layer streak instability in a turbulent channel flow with a lower curved wall, Marquillie *et al.*[58] use a streak extraction procedure based on a detection function expressed by Lin *et al.*[59] and an averaging process. Marquillie *et al.*[58] provide thus some evidence on the relationship between the turbulent kinetic energy production and the onset of secondary streak instability. The investigation of such a procedure for the logarithmic region could be also an interesting perspective.

ACKNOWLEDGMENTS

I would like to thank D. Biau for fruitful discussions on this topic and the two anonymous referees for their suggestions and helpful comments.

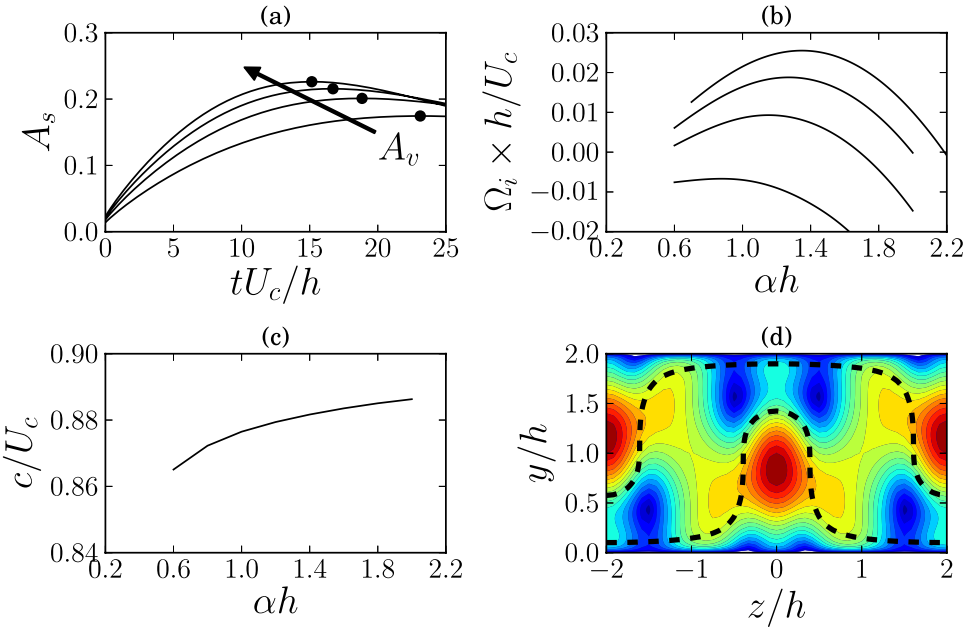

FIG. 15. Streak instability analysis for $Re_\tau = 300$ and $\beta h = \pi/2$. (a) Streak amplitudes *vs* time, scaled in outer units (h and U_c) for $A_v = 0.06,\ 0.078,\ 0.09$, and 0.1. The maximum amplitudes are denoted by •. (b) Temporal amplification rates *vs* the streamwise wavenumber, scaled in outer units for $A_s = 0.175,\ 0.2,\ 0.22$, and 0.23. (c) The phase velocity *vs* the streamwise wavenumber, scaled in outer units for $A_s = 0.2$. (d) Cross-stream view of the absolute value of the spanwise velocity component of the most amplified mode associated with $A_s = 0.23$ (i.e., $\alpha h = 1.3$). The contours levels are similar to those displayed in Figure 5(c).

APPENDIX: VALIDATION OF THE NUMERICAL APPROACH

In order to validate the present numerical approach, the instability of large scale optimal streaks (i.e., associated with the outer region) in turbulent channel flow is analyzed for the same flow conditions used by Park *et al.*,[38] namely, $Re_\tau = 300$ and $\beta h = \pi/2$. The computations are carried out with $N_y \times N_z = 151 \times 48$. Results are summarized in Figure 15. In panel (a), we show the temporal evolution of the streak amplitudes A_s for various amplitudes of the optimal initial vortices. The maximum amplitude for $A_v = 0.06,\ 0.078,\ 0.09$, and 0.1 are $A_s = 0.175,\ 0.2,\ 0.22$, and 0.23 which are very close to values given by Park *et al.*[38] ($0.18,\ 0.21,\ 0.23$, and 0.25, respectively). In panels (b) and (c), the distribution of the temporal amplification rate and the phase velocity are shown as a function of the streamwise wavenumber αh for $A_s = 0.175,\ 0.2,\ 0.22$, and 0.23. We obtain $\alpha h = 1.1$ for neutral conditions and a phase velocity $c/U_c \approx 0.87$ and 0.88. Despite a slight shift in temporal amplification rates, our results are consistent with those given by Park *et al.*[38] ($\alpha h = 1.2$ and $c/U_c = 0.87$). Finally, the cross-stream view of the absolute value of the spanwise velocity eigenfunction corresponding to $A_s = 0.23$ and $\alpha h = 1.3$ is shown in panel (d). The position of the critical layer is also reported. Once again, the mode shape is in close agreement with the one shown by Park *et al.*[38]

[1] T. Theodorsen, *The Structure of Turbulence* (The Institute for Fluid Dynamics and Applied Mathematics, University of Maryland, 1954).
[2] B. J. Cantwell, "Organized motion in turbulent flow," Annu. Rev. Fluid Mech. **13**, 457–515 (1981).
[3] R. J. Adrian, "Hairpin vortex organization in wall turbulence," Phys. Fluids **19**, 041301 (2007).
[4] S. J. Kline, W. C. Reynolds, F. A. Schraub, and P. W. Runstadler, "The structure of turbulent boundary layers," J. Fluid Mech. **30**, 741–773 (1967).
[5] H. T. Kim, S. J. Kline, and W. C. Reynolds, "The production of turbulence near a smooth wall in a turbulent boundary layer," J. Fluid Mech. **50**, 133–160 (1971).
[6] A. Townsend, *The Structure of Turbulent Shear Flow*, 2nd ed. (Cambridge University Press, 1976).
[7] A. E. Perry and M. S. Chong, "On the mechanism of turbulence," J. Fluid Mech. **119**, 173–217 (1982).
[8] A. E. Perry, S. Henbest, and M. S. Chong, "A theoretical and experimental study of wall turbulence," J. Fluid Mech. **165**, 163–199 (1986).

[9] I. Marusic, J. P. Monty, M. Hultmark, and A. J. Smits, "On the logarithmic region in wall turbulence," J. Fluid Mech. **716**, R3-1–R3-11 (2013).
[10] T. B. Nickels, I. Marusic, S. Hafez, and M. S. Chong, "Evidence of the k_1^{-1} law in a high-Reynolds-number turbulent boundary layer," Phys. Rev. Lett. **95**, 074501 (2005).
[11] J. A. Sillero, J. Jiménez, and R. D. Moser, "One-point statistics for turbulent wall-bounded flows at Reynolds numbers up to $\delta^+ = 2000$," Phys. Fluids **25**, 105102 (2013).
[12] M. Lee and R. D. Moser, "Direct numerical simulation of turbulent channel flow up to $Re_\tau \approx 5200$," J. Fluid Mech. **774**, 395–415 (2015).
[13] O. Flores and J. Jiménez, "Hierarchy of minimal flow units in the logarithmic layer," Phys. Fluids **22**, 071704 (2010).
[14] J. Jiménez and P. Moin, "The minimal flow unit in near-wall turbulence," J. Fluid Mech. **225**, 213–240 (1991).
[15] J. M. Hamilton, J. Kim, and F. Waleffe, "Regeneration mechanisms of near-wall turbulence structures," J. Fluid Mech. **287**, 317–349 (1995).
[16] F. Waleffe, "On a self-sustaining process in shear flows," Phys. Fluids **9**, 883–900 (1997).
[17] R. L. Panton, "Overview of the self-sustaining mechanisms of wall turbulence," Prog. Aerosp. Sci. **37**, 341–383 (2001).
[18] J. Kim and J. Lim, "A linear process in wall-bounded turbulent shear flows," Phys. Fluids **12**, 1885 (2000).
[19] M. T. Landahl, "A note on an algebraic instability of inviscid parallel shear flows," J. Fluid Mech. **98**, 243–251 (1980).
[20] P. J. Schmid and D. S. Henningson, *Stability and Transition in Shear Flows* (Springer, 2001).
[21] J. C. del Alamo and J. Jiménez, "Linear energy amplification in turbulent channels," J. Fluid Mech. **559**, 205–213 (2006).
[22] C. Cossu, G. Pujals, and S. Depardon, "Optimal transient growth and very large-scale structures in turbulent boundary layers," J. Fluid Mech. **619**, 79–94 (2009).
[23] G. Pujals, M. Garci-Villalba, C. Cossu, and S. Depardon, "A note on optimal transient growth in turbulent channels flows," Phys. Fluids **21**, 01519 (2009).
[24] W. C. Reynolds and K. M. F. Hussain, "The mechanics of an organized wave in turbulence shear flow. Part 3. Theoretical models and comparisons with experiments," J. Fluid Mech. **52**, 263–288 (1972).
[25] K. M. Butler and B. F. Farrel, "Optimal perturbations and streak spacing in wall-bounded turbulent shear flow," Phys. Fluids **5**, 774–777 (1992).
[26] J. Jiménez, "How linear is wall-bounded turbulence?," Phys. Fluids **25**, 110814 (2013).
[27] W. Schoppa and F. Hussain, "Coherent structure generation in near-wall turbulence," J. Fluid Mech. **453**, 57–108 (2002).
[28] J. Jiménez, "Cascades in wall-bounded turbulence," Annu. Rev. Fluid Mech. **44**, 27–45 (2012).
[29] Y. Hwang and C. Cossu, "Self-sustained processes in the logarithmic layer of turbulent channel flows," Phys. Fluids **23**, 061702 (2011).
[30] Y. Hwang, "Statistical structure of self-sustaining attached eddies in turbulent channel flow," J. Fluid Mech. **767**, 254–289 (2015).
[31] J. C. del Alamo, J. Jiménez, P. Zandonade, and R. D. Moser, "Self-similar vortex clusters in the turbulent logarithmic region," J. Fluid Mech. **561**, 329–358 (2006).
[32] C. D. Tomkins and R. J. Adrian, "Spanwise structure and scale growth in turbulent boundary layers," J. Fluid Mech. **490**, 37–74 (2003).
[33] I. Marusic and N. Hutchins, "Study of the log-layer structure in wall turbulence over a very large range of Reynolds number," Flow, Turbul. Combust. **81**, 115–130 (2008).
[34] Y. Hwang and C. Cossu, "Linear non-normal energy amplification of harmonic and stochastic forcing in the turbulent channel flow," J. Fluid Mech. **664**, 51–73 (2010).
[35] R. Moarref, A. S. Sharma, J. A. Tropp, and B. J. McKeon, "Model-based scaling of the streamwise energy density in high-Reynolds-number turbulent channels," J. Fluid Mech. **734**, 275–316 (2013).
[36] F. Alizard, S. Pirozzoli, M. Bernardini, and F. Grasso, "Optimal transient growth in compressible turbulent boundary layers," J. Fluid Mech. **770**, 124–155 (2015).
[37] A. S. Sharma and B. J. McKeon, "On coherent structure in wall turbulence," J. Fluid Mech. **728**, 196–238 (2013).
[38] J. Park, Y. Hwang, and C. Cossu, "On the stability of large-scale streaks in turbulent Couette and Poiseuille flows," C. R. Méc. **339**, 1–5 (2011).
[39] S. B. Pope, *Turbulent Flows* (Cambridge University Press, 2000).
[40] R. D. Cess, "A survey of the literature on heat transfer in turbulent tube flow," Westinghouse Research Report No. 8-0529-R24, 1958.
[41] W. C. Reynolds and W. G. Tiederman, "Stability of turbulent channel flow, with application to Malkus's theory," J. Fluid Mech. **27**, 253–272 (1967).
[42] S. Hoyas and J. Jiménez, "Scaling of the velocity fluctuations in turbulent channels up to $Re_\tau = 2003$," Phys. Fluids **18**, 011702 (2006).
[43] F. Alizard, J.-C. Robinet, and G. Filliard, "Sensitivity of optimal transient growth for turbulent boundary layer," Eur. J. Fluid Mech. **49**, 373–386 (2015).
[44] R. Peyret, *Spectral Methods for Incompressible Viscous Flow* (Springer, 2002).
[45] R. B. Lehoucq, D. C. Sorensen, and C. Yang, *ARPACK User's Guide: Solution of Large Scale Eigenvalue Problems with Implicitly Restarted Arnoldi Methods* (Society for Industrial & Applied Mathematics, 1997).
[46] P. Anderson, L. Brandt, A. Bottaro, and D. S. Henningson, "On the breakdown of boundary layer streaks," J. Fluid Mech. **428**, 29–60 (2001).
[47] G. Taylor, "The spectrum of turbulence," Proc. R. Soc. A **164**, 476–490 (1938).
[48] C. Cossu and L. Brandt, "On Tollmien-Schlichting waves in streaky boundary layers," Eur. J. Fluid Mech. **23**, 815–833 (2004).
[49] J. P. Monty, N. Hutchins, H. C. H. Ng, I. Marusic, and M. S. Chong, "A comparison of turbulent pipe, channel and boundary layer flows," J. Fluid Mech. **632**, 431–442 (2009).
[50] B. J. Balakumar and R. J. Adrian, "Large- and very-large-scale motions in channel and boundary-layer flows," Philos. Trans. R. Soc., A **365**, 665–681 (2007).

[51] W. M. F. Orr, "The stability or instability of the steady motions of a perfect liquid and of a viscous liquid. Part I: A perfect liquid. Part II: A viscous liquid," Proc. R. Irish Acad. A **27**, 9–68 (1907), available at www.jstor.org/stable/20490590.
[52] S. Pirozzoli and M. Bernardini, "Turbulence in supersonic boundary layers at moderate Reynolds number," J. Fluid Mech. **688**, 120–168 (2011).
[53] J. Hoepffner, L. Brandt, and D. S. Henningson, "Transient growth on boundary layer streaks," J. Fluid Mech. **537**, 91–100 (2005).
[54] M. Cossu, C. Chevalier, and D. S. Henningson, "Optimal secondary energy growth in a plane channel flow," Phys. Fluids **19**, 058107 (2007).
[55] C. Cossu, L. Brandt, S. Bagheri, and D. S. Henningson, "Secondary threshold amplitudes for sinuous streak breakdown," Phys. Fluids **23**, 074103 (2011).
[56] M. J. P. Hack and T. A. Zaki, "Streaks instabilities in boundary layers beneath free-stream turbulence," J. Fluid Mech. **741**, 280–315 (2014).
[57] N. J. Vaughan and T. A. Zaki, "Stability of zero-pressure-gradient boundary layer distorted by unsteady Klebanoff streaks," J. Fluid Mech. **681**, 116–153 (2011).
[58] M. Marquillie, U. Ehrenstein, and J. P. Laval, "Instability of streaks in wall turbulence with adverse pressure gradient," J. Fluid Mech. **681**, 205–240 (2011).
[59] J. Lin, J. P. Laval, J. M. Foucaut, and M. Stanislas, "Quantitative characterization of coherent structures in the buffer layer of near-wall turbulence," Exp. Fluids **45**, 999–1013 (2008).